# Spectral and statistical evaluation of the properties of the vibration measured at the base of an automotive seat for non-Gaussian random noise synthesis

**D. González** [1], **R. López-Valcarce** [2]
[1] CTAG, Acoustics and Vibration Laboratory,
Pol. Ind. A Granxa, 249-250, 36400 Porriño, Spain
e-mail: **damian.gonzalez@ctag.com**

[2] University of Vigo, Department of Signal Theory and Communications,
Campus Lagoas-Marcosende, Rúa Maxwell, 36310 Vigo, Spain

## Abstract
In this paper, we explore the properties of the vibration measured at the base of the driver seat when driving through different surfaces, with the purpose of defining a model for non-Gaussian random vibration testing. The recorded acceleration signals are first transformed to a 6 Degree of Freedom (DOF) space, and then segmented into stationary sections that are later analyzed. The non-Gaussian nature of the recorded vibration is demonstrated through different Gaussianity hypothesis tests, and the distribution of the third and fourth-order moments, as well as the crest factor, are computed and analyzed. The second-order spectral content reveals significant correlation at specific frequencies, while the significance of third-order polyspectra is checked through hypothesis testing. Based on our observations, a practical specification of the random process is proposed based on second-order spectral content, univariate kurtosis and crest factor levels.

## 1 Introduction

The usage of random vibration in mechanical testing of automotive components is a common technique, and has been applied in laboratories since many decades for the simulation of road-induced vibration. The spread of high-performance digital controllers allows accurate and repeatable control of Gaussian vibration profiles with desired power spectral density. One of the main advantages of using normal distributions is its solid theoretical foundations and the fact that many natural phenomena are well modelled through such distribution. Additionally, it is well known that a Gaussian stochastic process is completely characterized by its first and second-order statistics [1], *i.e.* mean and covariance. For a Gaussian zero-mean wide sense stationary (WSS) process, it suffices to give its autocorrelation sequence (or, equivalently, the coherence and variance). The spectral properties are then given by the Fourier transform of the autocorrelation function, which provides a convenient method for specifying the test conditions by means of the Power Spectral Density (PSD) or the Spectral Density Matrix (SDM), depending if the process is univariate or multivariate.

More recently, the focus in random vibration has moved to non-Gaussian processes, since field data suggests that significant deviation from Gaussianity can occur in many components, impacting its performance [2]. This results in higher complexity of the theoretical treatment and definition of the vibration problem. For non-Gaussian processes, the correlation function is not sufficient for fully characterising the process. A general definition must hence include the higher-order statistics (HOS), which consider the process statistics of order 3 and greater. As described in [3], these statistics are usually evaluated through the process cumulants and their Fourier transforms, known as polyspectra, which can be considered an extension of the second-order correlation function and classical power spectrum, respectively, to higher-orders. In general, the cumulants

for processes close to Gaussianity will be very small [3]. From a practical point of view, the usage of higher-order statistics for the definition of the non-Gaussian process has the following drawbacks:

1. Estimation of the second-order statistics (autocorrelation or power spectrum) with sufficient accuracy requires rather long signals, which is usually an issue due to the limited length of the test tracks used for the recording of the vibration signals, as well as to the lack of stationarity. This is even worse in the case of Multiple-DOF (MDOF) scenarios where, depending on the existing coherence between the different DOFs, the required record length for a given estimation accuracy may increase significantly. The estimation of the higher-order cumulants and polyspectra would require even larger records [3].

2. The complexity of the resulting model increases substantially. From an already large model consisting of a spectral density matrix (SDM) and joint first order probability density function (*pdf*), a new array would need to be introduced for each new HOS. In addition, the successive arrays will increase their dimensionality (second-order SDM is $N \times N$, third-order bispectrum is $N \times N \times N$, etc., with $N$ the number of DOFs).

A simpler approach consists in specifying the non-Gaussian process through its moments, although, in general, many different distributions may fit a particular set of moments. Clearly, there is a trade-off between the degree of accuracy when specifying a statistical model and the resulting complexity and effort during the specification stage. For this reason, it is important to have an adequate understanding of the statistical properties of real-world vibration signals, in order to determine which ones are truly significant and should be considered when specifying the model.

In this paper we evaluate the spectral and statistical properties of the input vibration to the driver seat of a car, in order to explore a practical specification of the non-Gaussian vibration process. First, the measurement setup is described. Then, the post-processing of the recorded signals is presented, including the transformation to a 6-DOF space and the extraction of stationary segments from the data. A statistical analysis of the extracted segments is later performed, including the evaluation of Gaussianity and of the third and fourth-order normalized moments and crest factor. The process correlation and the joint distribution of the MDOF process are also evaluated. Finally, a spectral analysis is performed, with a focus in the bispectral content of the process. Based on our analyses, a proposal for the specification of the non-Gaussian multivariate process and the conclusions complete this paper.

## 2 Measurement setup

The measured vehicle is a VW Scirocco, with the characteristics shown in table 1.

| Version | R-Line | Tyre | 205/50 R17 93V |
|---|---|---|---|
| Engine | 2.0 TDI | Front suspension | MacPherson strut |
| Gearbox | 6 gear DSG | Rear suspension | Four-link |

Table 1: Main vehicle characteristics.

The component selected for the measurements is the driver seat of the car. The acceleration input to the seat is recorded at the four fixing points with triaxial accelerometers, schematically shown in figure 1. This gives an overdetermined solution to the kinematics of the rigid body.

The fixing points of the seat are located symmetrically, which allows for the calculation of the Input Transform Matrix (ITM) from two distances, as indicated in figure 1. The specific values for the implemented instrumentation are 165 mm for length a, and 218.5 mm for length b.

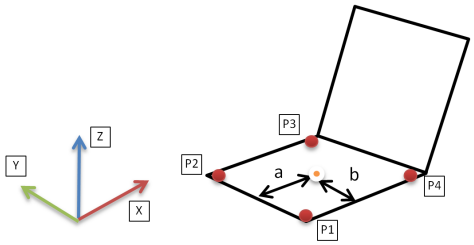


Figure 1: Location of the accelerometers.

The accelerometers used for the measurement are high sensitivity low mass ICP triaxial sensors (B&K type 4525 B and type 4535 B 001). A total of 12 acceleration signals, 5 GPS data streams and a video file are recorded per measurement. All the signals were sampled at 9600 Hz, applying a $4^{th}$ order Butterworth antialiasing filter with a -1dB cut-off frequency of 1000 Hz. The data acquisition systems used for the data recording are two HBM QuantumX MX840A, with external Somat ICP conditioning units.

A total of 4 scenarios are defined for measurement, as indicated in table 2. Most of the measured roads have sections of pavement in bad, fair and good condition. The roads used for the measurements are public roads. Hence, stability in the driving conditions was not guaranteed, and was subjected to the existing traffic.

| Scenario | Surface | Road type | Average speed (km/h) | Length (km) |
|---|---|---|---|---|
| A | Asphalt | Highway | 110 | 35.6 |
| B | Asphalt | Conventional | 52.5 | 124.2 |
| C | Concrete | Conventional | 70 | 4.2 |
| D | Cobblestone | Town | 30 | 0.5 |

Table 2: Measurement scenarios.

# 3 Signal post-processing

## 3.1 DOF transformation

The total 12 DOF measured at four points in X, Y and Z can be reduced to 6 DOF (X, Y, Z, Roll, Pitch and Yaw) without losing any information about the kinematics of the measured body. The transformation is performed through the Input Transform Matrix $[\mathcal{I}]$ [4], whose calculation is based on the distances shown in figure 1. The matrix $[\mathcal{I}]$ is computed so that the 6 DOF signals are obtained at the geometric center of the four measured points.

Figure 2 shows one of the recorded signals after transformation to the 6 DOF space. The transformation from a 12 DOF space to a 6 DOF space allows for halving the amount of data for post-processing.

## 3.2 Signal segmentation

Figure 2 illustrates the fact that the vibration process is in general non-stationary, although it can be considered approximately stationary over sufficiently short periods of time. Therefore, stationary segments are first extracted. The criterion for the segmentation is the extraction of the largest possible blocks of samples that can be considered stationary based on different statistical tests. For such purpose, an algorithm based on k-means clustering of the constant percentage bandwidth (CPB) spectra has been developed and applied

[5]. The segments of duration below 10 seconds, or with at least one of the blocks in the segment having null associated vehicle speed, or an average vehicle speed of the segment under 10 km/h, are all discarded.

Figure 2 illustrates the result of the segmentation for one of the measurements. The regions that were not assigned to a stationary segment are indicated in blue, while the different stationary segments are shown in different colors. The percentage of the total recorded signal that is retained after segmentation is 33%, the rest 67% being associated with transients. The supposedly stationary segments retained in this way are in general quite short, with most of them having durations under 20 seconds.

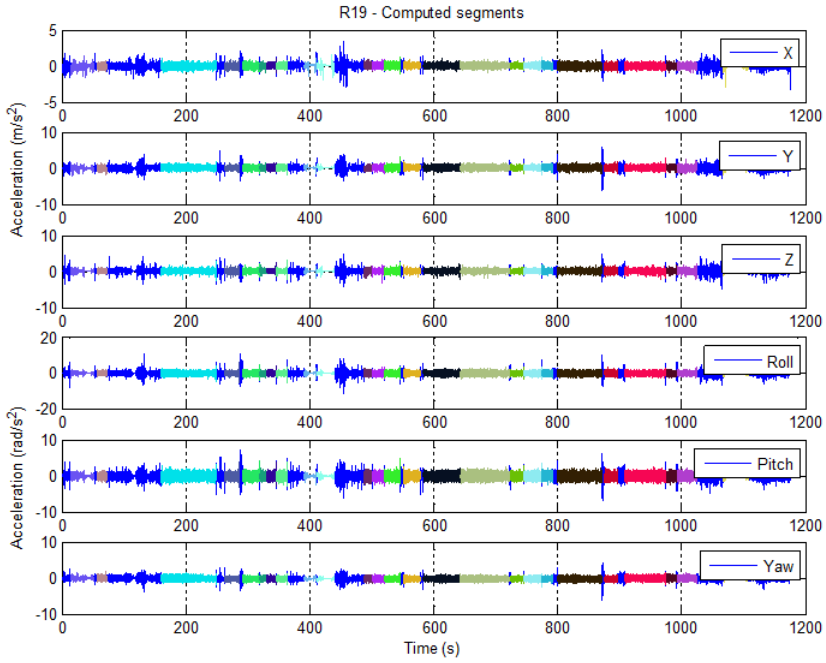


Figure 2: Result of the segmentation of one of the recordings. The regions not assigned to a stationary segment are shown in blue. The rest of the colors correspond to different segments extracted.

After the segmentation of the signals, two different stationarity tests are applied to each segment: runs test [6] and reversals test [6]. All these tests are applied individually to each of the 6 DOFs of the transformed process. A segment is considered stationary if all 6 DOFs pass the stationarity test.

Table 3 shows the percentage of segments passing stationarity tests respect to the total recorded signal, depending on the number of tests passed. Most of the recorded data corresponds to non-stationary segments and segments with no vibration. About 25% of the whole recordings, and nearly 80% of the extracted segments pass at least one of the stationarity tests while half of them pass both.

| Description | Duration | Percentage of total duration | Percentage of extracted duration |
|---|---|---|---|
| Total length | 3:52:14 | 100% | — |
| Extracted length | 1:16:43 | 33% | 100% |
| Stationary 2 crit. | 0:30:36 | 13% | 40% |
| Stationary 1 crit. | 1:00:43 | 26% | 79% |

Table 3: Percentage of stationary segments depending on the number of stationarity tests that do not reject the stationarity null hypothesis, for a significance level of 0.05.

### 3.3 Gaussianity assessment

The assessment of the Gaussianity of each segment is done through four different tests: chi-squared [1], skewness, kurtosis and BHEP (Baringhaus-Henze-Epps-Pulley) [7] [8].

The univariate tests are applied to each DOF individually, and, for a given test, the process is considered Gaussian if all the DOFs pass the test. This does not imply that the process is jointly normal (counterexamples can be found in [1]). This latter condition is tested through the BHEP test, which is applied to the 6 DOF process. Table 4 shows the total cumulative duration of the segments that passed the different tests, as well as the percentage of duration of the extracted segments that pass the Gaussianity test. Although some DOFs in some segments can be considered Gaussian, in general the process fails to pass the tests. In particular, none of the extracted segments passes the multivariate BHEP test, evidencing the lack of Gaussianity of the process.

| DOFs | Chi-squared | | Skewness | | Kurtosis | | BHEP | |
|---|---|---|---|---|---|---|---|---|
| | Duration | % | Duration | % | Duration | % | Duration | % |
| 1 | 0:11:56 | 16% | 0:15:07 | 20% | 0:12:22 | 16% | — | — |
| 2 | 0:08:37 | 11% | 0:17:24 | 23% | 0:04:19 | 6% | — | — |
| 3 | 0:06:23 | 8% | 0:18:07 | 24% | 0:04:23 | 6% | — | — |
| 4 | 0:04:15 | 6% | 0:11:21 | 15% | 0:01:32 | 2% | — | — |
| 5 | 0:00:00 | 0% | 0:05:37 | 7% | 0:00:00 | 0% | — | — |
| 6 | 0:00:21 | 0% | 0:00:22 | 0% | 0:00:00 | 0% | 0:00:00 | 0% |

Table 4: Total cumulative duration of segments that pass the Gaussianity tests. The DOFs column indicate the number of DOFs that pass the test. The percentage columns correspond to the proportion of the duration of the extracted stationary segments that pass the test, for a significance level of 0.05.

## 4 Distribution of the moments and crest factor of the process

Since the process cannot be considered strictly Gaussian, we will now evaluate the statistical properties of the segments in order to check how distant from a normal distribution they are. Since moments of order 3 and 4 are fixed for a Gaussian process, we will focus on the skewness and kurtosis, defined as the third and fourth standardized moments. The first measures the asymmetry of the distribution, while the later quantifies the relative height of the tails.

$$\gamma = \mathbb{E}\left\{\left(\frac{X-\mu}{\sigma}\right)^3\right\} = \frac{\mathbb{E}\left\{(X-\mu)^3\right\}}{(\mathbb{E}\left\{(X-\mu)2\right\})^{3/2}} \tag{1}$$

$$\beta = \mathbb{E}\left\{\left(\frac{X-\mu}{\sigma}\right)^4\right\} = \frac{\mathbb{E}\left\{(X-\mu)^4\right\}}{(\mathbb{E}\left\{(X-\mu)^2\right\})^2} \tag{2}$$

Given the samples $\{x[n], n = 1, ..., N\}$, the sample skewness is computed as follows:

$$\hat{\gamma} = \frac{\sqrt{N(N-1)}}{N-2} \cdot \frac{\frac{1}{N}\sum_{n=1}^{N}(x[n]-\hat{m}_1)^3}{\left(\sqrt{\frac{1}{N}\sum_{n=1}^{N}(x[n]-\hat{m}_1)^2}\right)^3} \tag{3}$$

with $\hat{m}_1$ the sample mean. The estimator $\hat{\gamma}$ is unbiased [9]. As for the sample kurtosis, we have the following biased estimator:

$$\hat{\beta}_b = \frac{\frac{1}{N}\sum_{n=1}^{N}(x[n]-\hat{m}_1)^4}{\left(\frac{1}{N}\sum_{n=1}^{N}(x[n]-\hat{m}_1)^2\right)^2} \tag{4}$$

An unbiased alternative can be computed as [9]:

$$\hat{\beta}_u = \frac{N-1}{(N-2)(N-3)}\Big((N+1)\hat{\beta}_b - 3(N-1)\Big) + 3 \tag{5}$$

For the analysis of these two moments, we used the unbiased estimators.

It is well known that the variance of the sample estimators depends on the number of samples used for the estimation. Formulas are available that relate this variance to the number of samples under the assumption of independence between samples. In our case, the process is low-pass, which means that the samples are not independent. Under the assumption of weak dependence, we can compute a confidence interval for the sample estimators through the stationary bootstrap [10]. The values given here correspond to a coverage factor of K = 0.95.

## 4.1 Skewness

The histogram of the signal duration for different skewness levels is shown in figure 3. The skewness is estimated from all the samples within each segment, and only those passing at least one stationarity test are included in this analysis. These graphs confirm the fact that the skewness is most of the time very close to 0, showing a larger dispersion for the X and Z DOFs.

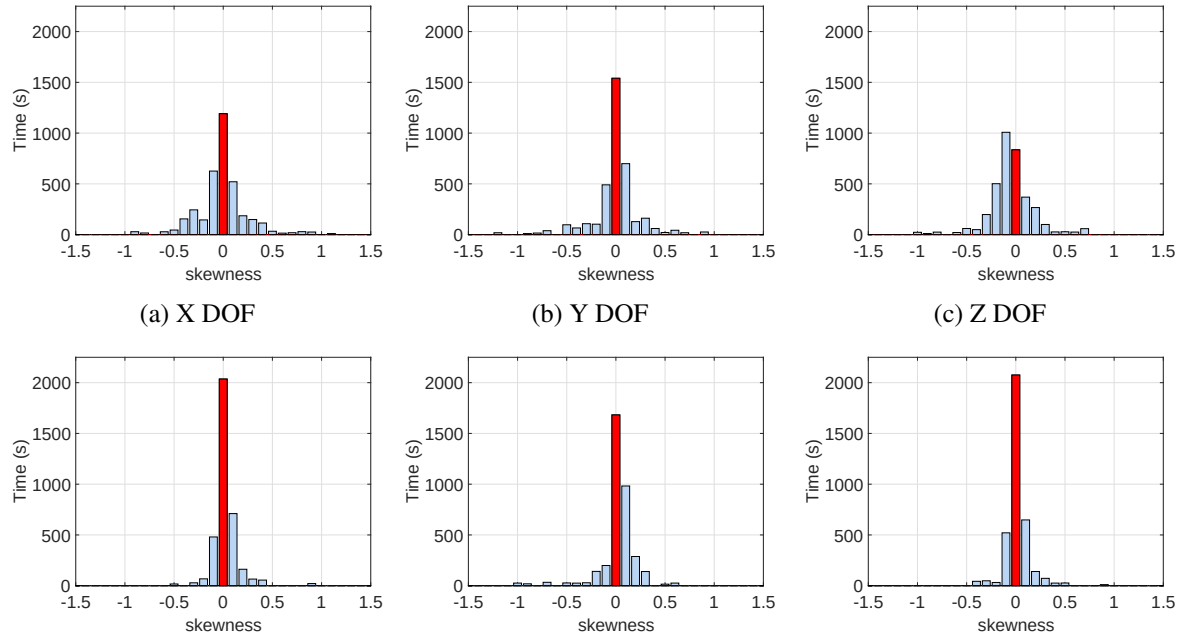


(a) X DOF (b) Y DOF (c) Z DOF

(d) Roll DOF (e) Pitch DOF (f) Yaw DOF

Figure 3: Total duration of stationary recorded signal for different skewness levels and DOFs. The Gaussian skewness level is highlighted in red.

Figure 4 shows the distribution of the size of the confidence interval of the skewness estimate as a function of the segment size. The uncertainty in the estimation of the skewness increases mainly with small segments. It is worth noting the significant level of uncertainty in the estimation for some of the segments, which

is reasonable taking into account the fact that the skewness is a third-order moment and the process is coloured. This has some practical implications, meaning that care must be exercised when considering a certain skewness level based on short recordings.

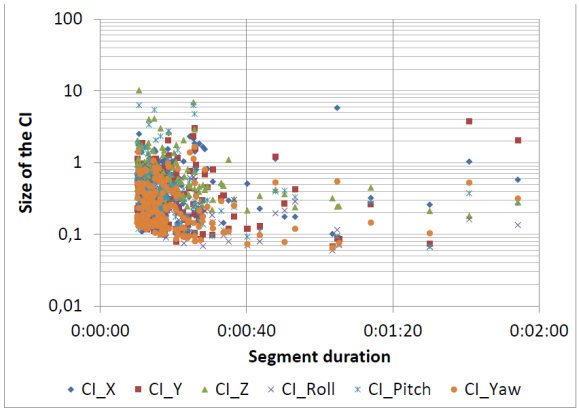


Figure 4: Size of the confidence interval of the skewness sample estimate, as a function of the segment size, computed through the stationary bootstrap for a coverage factor of 95%.

## 4.2 Kurtosis

The distribution of the kurtosis level is shown in figure 5 for the different DOFs. As for the skewness, only the segments passing at least one stationarity test are included in this analysis. This graph confirms the fact that most of the recorded signals are very close to Gaussianity in terms of its kurtosis, although the distribution is skewed to the right, indicating that the values tend in general to be larger than for the Gaussian distribution. There is also a clear difference among the measured DOFs. There is a prevalence of large kurtosis values in Z direction, which is reasonable since it is the main direction of vibration input to the car. In all the cases the kurtosis levels are mostly above 3, indicating a clear leptokurtic behaviour.

As with the skewness estimate, one possible cause for the large dispersion in the kurtosis values for small segments may be the variability in the estimator when few samples are available. For small segment sizes (below 30 seconds) we find a significant increase in the distance between the upper and lower bounds of the confidence interval (CI). This can be observed in figure 6, showing the distribution of the size of the CI as a function of the segment size. The same shape as for the skewness is noticeable, indicating that the uncertainty in the estimation of the kurtosis increases mainly with small segments. Again, care must be exercised when considering a certain kurtosis level based on short recordings, due to the large uncertainty of the estimate under this condition.

## 4.3 Crest factor analysis

Although the Gaussian distribution is unbounded in the abscissa, real vibration processes are bounded due to physical constraints. This implies an additional deviation from Gaussianity in real-world processes, where the tails may present larger probabilities than the normal distribution, but will at a certain point fall to zero faster than normal. In practical vibration synthesis systems, for zero-mean processes this limitation is imposed through a signal clipping at a certain multiple of the standard deviation or RMS level, effectively limiting the crest-factor, but also producing a spectral distortion that can be compensated through post-filtering and closed-loop control techniques [11].

The crest factor (CF) of the stationary segments obtained from the field data is computed according to equation (6). The distribution of the CF is computed considering the duration of the road data, *i.e.*, the cumulative time with a CF in a certain range. The resulting histograms are shown in figure 7.

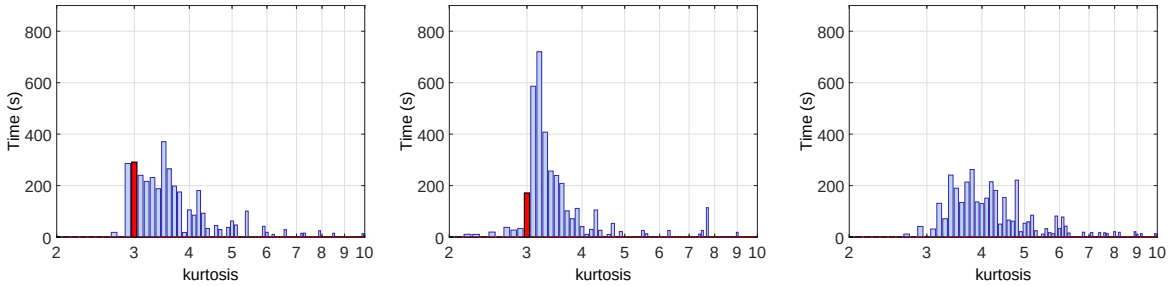


(a) X DOF (b) Y DOF (c) Z DOF

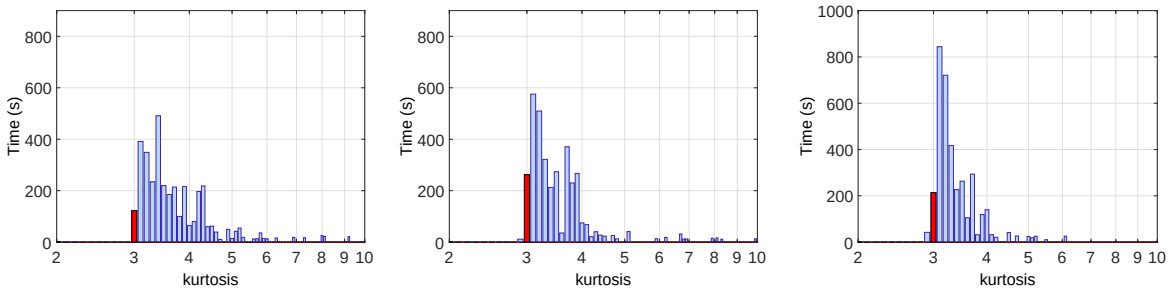


(d) Roll DOF (e) Pitch DOF (f) Yaw DOF

Figure 5: Total duration of stationary recorded signal for different kurtosis levels and DOFs. The Gaussian kurtosis level is highlighted in red.

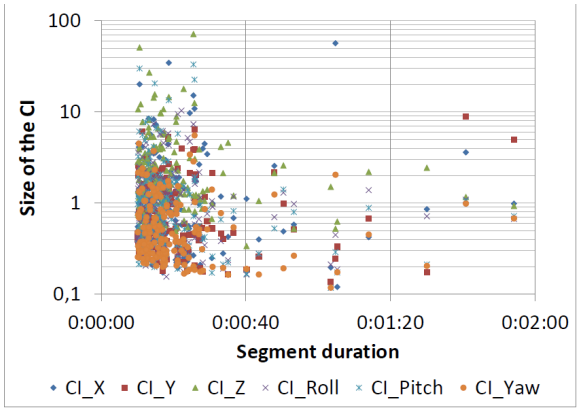


Figure 6: Size of the confidence interval of the kurtosis sample estimate, as a function of the segment size, computed through the stationary bootstrap for a coverage factor of 95%. Only segments that passed at least one stationarity test are shown.

$$\mathrm{CF} = \frac{|x|_{peak}}{x_{rms}} \tag{6}$$

In general, the CF spreads over a broad range starting close to 3 till more than 13. Most of the time the crest factor is near 5, which turns out to be a common CF for Gaussian random profile clipping in vibration testing, together with CF = 3.

From the previous analysis, it can be concluded that limiting the CF is a feature that is necessary if a realistic model of the vibration process is to be implemented, and should be considered also for random vibration tests using non-Gaussian processes.

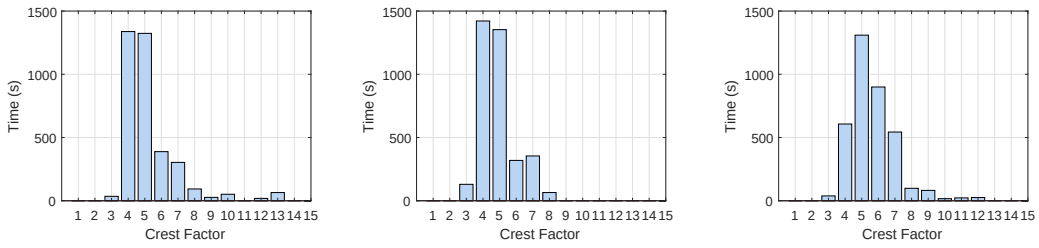


(a) X DOF (b) Y DOF (c) Z DOF

(d) Roll DOF (e) Pitch DOF (f) Yaw DOF

Figure 7: Total duration of stationary recorded signal for different crest factors (CF) and DOFs.

# 5 Marginal distributions

In this section we analyse the shape of the marginal distributions of the process. These probability density functions are estimated through the kernel density [12]. For better illustration, a histogram of the marginal distribution of the X, Y and Z DOF of the extracted segments is shown in figure 8. A similar result is obtained for the rotational DOFs (Roll, Pitch and Yaw). The following can be observed:

1. The *pdf* has a bell shape, clearly resembling a Gaussian distribution.
2. The distribution is different for each of the process DOFs. The tails of the marginal distribution for Z axis are significantly larger than for the X and Y axes, as shown in figure 8c, which is in agreement with the kurtosis values obtained for this axis in section 4.2.

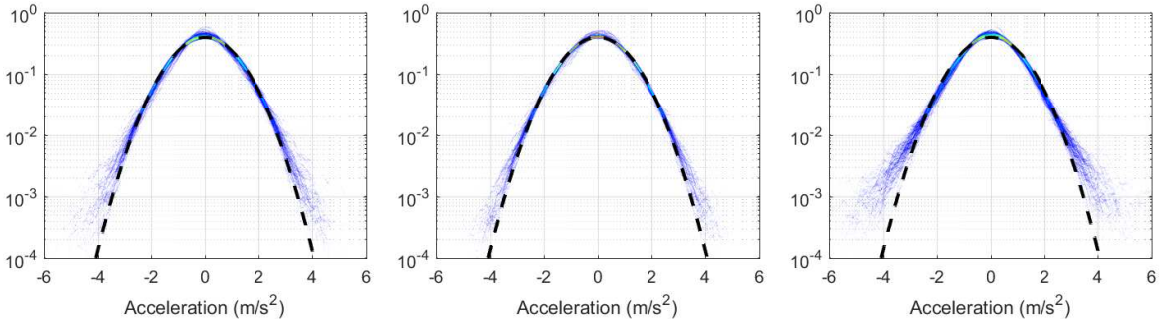


(a) X DOF (b) Y DOF (c) Z DOF

Figure 8: Histogram of the normalised kernel estimate of the marginal distribution of the X DOF (a), Y DOF (b) and Z DOF (c) for all extracted segments. The dashed line corresponds to the normal distribution.

# 6 Process correlation and joint distribution

Before evaluating any joint distribution of the process, it is of interest to check the level of correlation between the different DOFs. We will first compute the matrix of correlation coefficients for the transformed 6-DOF process. This allows for checking the degree of linear dependence between the process DOFs, without considering the time dependence (this will be done later). The correlation coefficient matrix is computed for the unsegmented recordings and is shown in table 5. The correlation coefficients are very small but for the Y and Yaw DOFs.

| **Signal** | **X** | **Y** | **Z** | **Roll** | **Pitch** | **Yaw** |
|---|---|---|---|---|---|---|
| X | 1.00 | 0.01 | -0.03 | -0.02 | -0.03 | 0.11 |
| Y | | 1.00 | -0.06 | 0.04 | -0.12 | -0.39 |
| Z | | | 1.00 | -0.10 | -0.04 | -0.10 |
| Roll | | | | 1.00 | 0.10 | 0.08 |
| Pitch | | | | | 1.00 | 0.05 |
| Yaw | | | | | | 1.00 |

Table 5: Average correlation coefficients matrix for the 6 DOF process.

The previous analysis can be repeated considering the correlation structure of the process in the frequency domain. A simple way for observing such correlation is the calculation of the coherence function, defined in equation (7), where $G_{xx}(f)$ is the autospectral density of $x$, $G_{yy}(f)$ the autospectral density of $y$ and $G_{xy}(f)$ their cross spectral density. According to this equation, given the autospectral density of the process, the coherence function can be used instead of the modulus of the cross-spectral density in the definition of the multivariate process. The Welch method is applied for the estimation of this function [6], using a Hanning window, spectral resolution of 1 Hz and no overlap.

$$C_{xy}(f) = \frac{|G_{xy}(f)|^2}{G_{xx}(f)G_{yy}(f)} \tag{7}$$

In order to get further insight in the range of coherence levels that can be found in this particular case, we can plot a 3D histogram of the coherence function computed for the extracted segments. The result is shown in figure 9 for three different cases. The first one corresponds to two DOFs clearly showing low coherence in all the frequency range. A bivariate process consisting of these two DOFs is likely to be well modelled through two uncorrelated univariate signals. In figure 9b, we can observe a scenario showing large coherence around 15 Hz, which means that lateral motion at that frequency will most probably be accompanied by a Roll movement. Although Y and Yaw DOFs present the largest average absolute correlation coefficient in table 5, coherence between those two DOFs is in general low, with larger values only at frequencies above 80 Hz.

From the data in this section, we can conclude that significant correlation among the process DOFs can exist, even for stiff measurement points such as the seat base. This aspect would not be considered with the usage of uncorrelated noise for the simulation of multiaxial vibration processes.

The evaluation of the joint density of the process is done through the inspection of the kernel density estimate. Unfortunately, the inspection of the joint density is difficult or practically impossible for more than 3 DOFs. We will give here some representative examples for the 2 and 3 DOF case.

The analysis of the 2-DOF joint distribution reveal that all the joint densities have a clear elliptical shape. This aspect is better observed in figures 10a and 10b, corresponding to a contour plot of the kernel density estimate for two different segments and signals. The first one shows a clear correlation between the two DOFs, while the second figure indicates a lower correlation level. Another significant aspect is the shape of the kernel estimate at the tails of the density. In figure 10a the lower level contours are not perfectly elliptical,

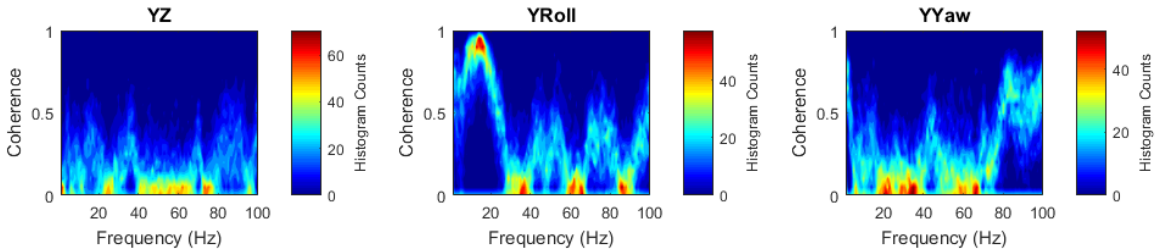


(a) (b) (c)

Figure 9: Ordinary coherence histogram for two DOFs mostly uncorrelated (a), with coherent behaviour near 15 Hz (b) and with coherent behaviour at high frequency (c).

being the segment 14 seconds long. This irregular shape is due to the reduced number of samples at the tails. In figure 10b, the duration increases to 87 seconds, which means a larger number of samples at the tails and hence a better definition of the lower level ellipses. This point is significant in relation to the accuracy of the joint density estimate for higher dimensions. The low probability of having a significant number of points at the tails of the distribution will lead to the need for large sequences for an adequate estimate. Hence, a non-parametric estimation might be discouraged due to the large errors that may exist.

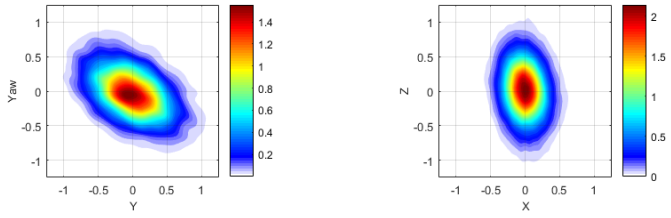


(a) (b)

Figure 10: 2-DOF joint density estimate for two different stationary segments.

The 3-DOF joint density is shown as a family of isosurfaces for one segment. Due to the large computational cost of the kernel density estimate for this number of DOFs, only two segments were evaluated in order to have an overview of the general shape of the distribution. The result is shown in figure 11. The same elliptical shape as for the bivariate case is observed. Now the tails are not as well defined as for the bivariate case. This is a consequence of the fact that, since the number of samples is limited, the number of them outside a certain isosurface reduces due to the larger available volume. That makes isolate kernels visible for the lowest level isosurface.

## 6.1 Process ellipticity

From the observation of the 2 and 3-DOF kernel density estimates, the process seems to have elliptical symmetry. In order to assess this property for different DOFs and larger dimensions, a multivariate ellipticity test is applied, based on [13]. The test is applied to each DOF separately, to a 3 DOF set consisting of $\{X, Y, Z\}$ and a 6 DOF set integrated by all available signals. The mean of the process is removed prior to the application of the test. In all cases a significance level of 0.05 is considered. For the case of individual DOFs, the test is unable to reject the null hypothesis of ellipticity. All the stationary segments under analysis present a symmetric distribution under univariate conditions. For the 3 DOF case, 45% of the duration of the stationary segments pass the ellipticity test, while the other 55% does not. Similar results are obtained for the 6 DOF case, with 44% of the signal duration passing the test, and 56% having the null hypothesis rejected.

A segment with rejected ellipticity and another one with the same hypothesis not rejected are evaluated

graphically in order to further analyse the overall shape of the estimated distribution. Both segments have a similar length. A kernel density estimate is performed for the 3-DOF case. Figures 11a and 11b show a 3D plot of the process distribution. From the observation of these graphs, no clear differences are noticeable that could indicate a lack of ellipticity of the analysed segments. This could indicate that the applied test might be too conservative when rejecting the ellipticity null hypothesis.

The results of the application of this ellipticity test are not conclusive, indicating that a significant percentage of the signal duration might present some amount of multivariate skewness.

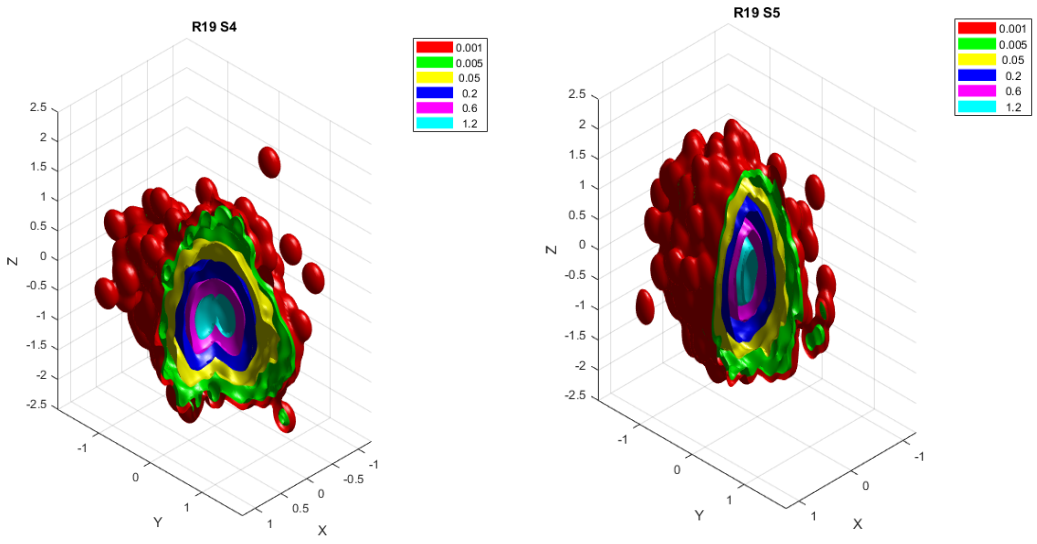


(a) (b)

Figure 11: 3-DOF kernel density estimate for a segment with rejected (a) and accepted (b) ellipticity.

# 7 Spectral analysis

The spectral content of Gaussian processes can be properly specified through the Spectral Density Matrix (SDM), which includes the second-order spectra. For a 6 DOF process, this involves the specification of a $6 \times 6$ matrix with 6 autospectra and 30 cross-spectra. The calculation and structure of the SDM is well known in the field of vibration testing and is not shown here for brevity.

One of the main difficulties of using non-Gaussian distributions when modelling a vibration process is the need of higher-order spectra for the proper definition of the process.

An exploratory evaluation of bispectra is done in order to verify the departure from Gaussianity based on this higher-order spectrum. The analysis is based on the work by Hinich [14], while the test is applied based on an implementation by A. Swami [15]. Since Hinich's test checks the null hypothesis of the bispectrum being zero, a failure in rejecting such null hypothesis would reinforce the idea of the bispectrum not being strictly necessary for a practical definition of the non-Gaussian MDOF vibration process.

The test is applied to each of the stationary segments extracted from the measured data. The percentage of segments whose bispectrum can be considered null is indicated in table 6.

For a large percentage of the signal duration, the hypothesis of the bispectrum being null can not be rejected. Only the Z DOF shows a 19% of the measured time having a significant bispectral level, being the rest of the DOFs below 10%. This result reinforces the idea of not considering the higher-order spectra in the specification of the non-Gaussian vibration process, since the additional effort required for the process specification would not likely provide significant improvements in terms of model accuracy.

| DOF | Total time | Hinich test | Fraction |
|---|---|---|---|
| X | 01:16:43 | 01:09:32 | 91% |
| Y | 01:16:43 | 01:11:20 | 93% |
| Z | 01:16:43 | 01:01:48 | 81% |
| Roll | 01:16:43 | 01:15:02 | 98% |
| Pitch | 01:16:43 | 01:14:07 | 97% |
| Yaw | 01:16:43 | 01:13:28 | 96% |

Table 6: Hinich Gaussianity test for a significance level of 0.05.

# 8 Specification of the process

Two approaches can be considered for the specification of the multivariate non-Gaussian process. The first one is based on a strong assumption of non-Gaussianity, which would require the definition of the higher-order spectra and statistics, as well as the joint density of the process. This seems to be impractical, particularly when field data suggests that some simplifications can be reasonably made on the model in order to significantly reduce the necessary modelling and analysis effort. The second, more practical specification of the process is based on the results presented in this paper. The following elements are considered as part of the model, and are summarized in table 7.

1. Spectral Density Matrix, including autospectra and cross-spectra. The modulus of the cross-spectra can be replaced by an estimate of the process coherence.
2. Higher-order statistics: the specification of the process kurtosis is considered sufficient for most of the actual road vibration scenarios. Skewness is found to be very close to zero. The crest factor can provide useful information about the tail decay of the process distribution. These parameters should be specified for all the relevant DOFs.

The higher-order spectra are not considered for the process model, due to the following reasons:

- It was shown that, for the extracted stationary segments, the bispectra can be considered null in most of the cases.
- The complexity of the model would increase significantly when including the HOS, becoming impractical.

| Property | Non-Gaussian | Proposed |
|---|---|---|
| SDM | Required | Required |
| Higher-order Spectra | Required | Not considered |
| Higher-order Statistics | Required | Univariate Kurtosis required. Skewness considered null. |
| Joint Density | Required | Not considered |
| Crest factor | Not required (implicit in joint density) | Recommended |

Table 7: Process specification considering requirements under strong non-Gaussian conditions, and proposed simplified specification.

# 9 Conclusions

This paper describes field measurements performed on a car seat, with the purpose of providing an empirical background and a set of parameters for the proper definition of a non-Gaussian random process for vibration testing. The recorded signals are segmented into stationary sections for later analysis. The non-Gaussian nature of the recorded vibration is demonstrated through different Gaussianity hypothesis tests. It is found that, in general, the skewness is very close to zero, whereas the kurtosis is larger than that of a Gaussian. The crest factor was shown to cover a broad range of values. The marginals present in general a leptokurtic distribution. The inspection of the kernel estimates of the 2 and 3 DOF densities reveals elliptical symmetries. The application of a pseudo-Gaussian ellipticity test was not conclusive in rejecting this hypothesis. The second-order spectral content reveals significant correlation at specific frequencies, while third-order polyspectra can most of the time be considered null, reinforcing the lack of polyspectra in the specification of the process. A practical specification of the process is proposed based on second-order spectral content, univariate kurtosis and crest factor levels.

# Acknowledgements

The work of R. López-Valcarce was partially funded by the Agencia Estatal de Investigación (Spain) and the European Regional Development Fund (ERDF) under project WINTER (TEC2016-76409-C2-2-R), and by the Xunta de Galicia (Agrupación Estratéxica Consolidada de Galicia accreditation 2016-2019; Red Temática RedTEIC 2017-2018) and the European Union (ERDF).

# References

[1] A. Papoulis, S.U. Pillai, *Probability, random variables, and stochastic processes*, McGraw-Hill, (2002).

[2] D.O. Smallwood, *Generation of partially coherent stationary time histories with non-Gaussian distributions*, Technical Report, Sandia National Labs., Albuquerque (United States), (1996).

[3] J.M. Mendel, *Tutorial on higher-order statistics (spectra) in signal processing and system theory: theoretical results and some applications*, Proceedings of the IEEE, Vol. 79, No. 3, IEEE (1991), pp. 278-305.

[4] N. Fitz-Coy, V. Nagabhushan, M.T. Hale, *Benefits and challenges of over-actuated excitation systems*, Shock and Vibration, Vol. 17, No.3, Hindawi Publishing Corporation (2010), pp. 285-303.

[5] D. González , *Segmentation based on k-means clustering of CPB spectra*, Technical Report, TR-010-2014-B, Universidade de Vigo, (2014).

[6] J.S. Bendat, A.G. Piersol, *Random Data: Analysis and Measurement Procedures*, John Wiley & Sons (2011).

[7] A. Madansky, *Prescriptions for working statisticians*, Springer, New York (1988).

[8] N. Henze, *Invariant tests for multivariate normality: a critical review*, Statistical papers, Vol. 43, No. 4, Springer (2002), pp. 467-506.

[9] D.N. Joanes, C.A. Gill, *Comparing measures of sample skewness and kurtosis*, Journal of the Royal Statistical Society: Series D (The Statistician), Vol. 47, No. 1, Wiley (1998), pp. 183-189.

[10] D.N. Politis, J.P. Romano, *The stationary bootstrap*, Journal of the American Statistical Association, Vol. 89, No. 428, Taylor & Francis Group (1994), pp. 1303-1313.

[11] A. Steinwolf, *Shaker random testing with low kurtosis: Review of the methods and application for sigma limiting*, Shock and Vibration, Vol. 17, No. 3, Hindawi Publishing Corporation (2010), pp. 219-231.

[12] B.W. Silverman, *Density estimation for statistics and data analysis*, Chapman and Hall/CRC (1986)

[13] D. Cassart, *Optimal Tests for Symmetry*, PhD Thesis, Université Libre de Bruxelles (2007).

[14] M.J. Hinich, *Testing for Gaussianity and linearity of a stationary time series*, Journal of time series analysis, Vol. 3, No. 3, Wiley (1982), pp. 169-176.

[15] A. Swami, J.M. Mendel, C.L.M. Nikias, *Higher-order spectral analysis toolbox*, United Signals & Systems, Inc. (1993).